

Discovery of differential equations using sparse state and parameter regression

Teddy Meissner ^{*} and Karl Glasner [†]

June 12, 2024

Abstract

This paper proposes a sparse regression strategy for discovery of ordinary and partial differential equations from incomplete and noisy data. Inference is performed over both equation parameters and state variables using a statistically motivated likelihood function. Sparsity is enforced by a selection algorithm which iteratively removes terms and compares models using statistical information criteria. Large scale optimization is performed using a second-order variant of the Levenberg-Marquardt method, where the gradient and Hessian are computed via automatic differentiation. Illustrations involving canonical systems of ordinary and partial differential equations are used to demonstrate the flexibility and robustness of the approach. Accurate reconstruction of systems is found to be possible even in extreme cases of limited data and large observation noise.

1 Introduction

Combining fundamental physical laws with observational data is an ongoing scientific challenge. Whereas differential equations derived entirely from first principles have been broadly successful in basic physics and mechanics, this approach is insufficient for complex systems ranging from materials science to biology. In those cases, model development involves a variety of phenomenological assumptions, which must be calibrated or verified from observations. Many recent efforts have focused on the problem of sparse model discovery, which involves generating equations from scratch that attempt to balance trade-offs between fitting data, parsimony, and interpretability of the discovered model.

Historically, the earliest methods of combining data and differential equations were concerned with the inverse problem of parameter estimation (e.g. [51] and references therein). Traditional least squares regression, penalizing the difference between model output and data, has been used successfully for parameter estimation in differential equations [18, 1, 4, 19, 28, 15, 49, 57, 68, 21]. Alternatively, optimizing over the residual error can be used instead [49, 11, 25, 34, 12, 54]. Methods which simultaneously infer the state and parameter variables combine these two approaches [50, 64, 22], and have proven to be more robust for handling noisy and incomplete data. Gaussian process regression [46, 47] has also been proposed for parameter estimation. Lastly, a variety of studies employ Bayesian inference (e.g. [16, 6, 66, 68, 67]) that provides a detailed probability distribution of parameter values, which is useful for tasks such as uncertainty quantification.

Discovering differential equations from data, rather than estimation of parameters in a known model, has seen a surge of interest, but has less theoretical underpinnings. Some of the earliest work in this direction involves symbolic regression [8, 55]. These procedures consist of generating candidate equations by symbolically combining elementary operations, and testing them competitively to ensure a good fit with the data. A variety of extensions build upon this idea, employing either genetic algorithms or deep learning strategies [36, 63, 5, 40, 13].

^{*}Corresponding Author: Program in Applied Mathematics, University of Arizona, Tucson AZ 85721 USA

[†]Department of Mathematics, University of Arizona, Tucson AZ 85721 USA

An alternative to symbolic discovery involves regression with a given set of candidate terms, or at least a general equation structure. In order to identify models which are both parsimonious and do not overfit data, these methods rely on promoting sparsity in the parameter set. This can be accomplished by using statistical information criteria [38], L^1 penalization [54], or a sequential thresholding algorithm (“SINDy”) [12, 53]. These studies rely on residual regression, which is notoriously sensitive to noisy data, and cannot intrinsically handle incomplete data. Proposals to ameliorate these problems involve utilizing weak integral formulations, where the equations are replaced with inner products over test functions [52, 41]. Sparsity has also been incorporated into Bayesian versions of model discovery [9, 27].

It has become increasingly popular to employ neural network function approximation [7, 48] instead of traditional grid-based or finite element representations. These “physics-informed” machine learning methods [29] rely on a loss function similar to hybrid regression methods discussed above, inferring both the solution and parameters. They have been adapted to model discovery by including a sparsity-inducing penalty term in the loss function, and search for equations composed of predefined library terms [10, 65] or represented by rational neural networks [60, 59]. Alternatively, neural networks may be employed to approximate the right hand side of a system directly [31, 26].

This paper introduces a method for sparse regression which is based upon simultaneous inference of both parameters and state variables. This contrasts to regression methods that only infer parameters either by penalizing the difference between data and model output (e.g. [51]), or the residual error (e.g. [49, 54, 12, 53]). This mixed regression approach on one hand ameliorates difficulties with non-convex optimization [21], and on the other is very robust for noisy data [51, 22]. Our approach is formulated with generality in mind, and applies to algebraic systems as well as ordinary and partial differential equations. This paper’s examples focus on the latter, and utilize conventional finite difference approximations, although this is not a necessary restriction, as any finite dimensional function representation could be used. Sparsity of the parameter set is selected by classical information criteria, together with a parameter pruning algorithm that relies on a regularized l_0 penalty. Our results illustrate the flexibility and robustness of the approach in accurately identifying systems even in cases of limited data and large observation noise.

This paper is structured as follows: formulation of our regression strategy and its statistical underpinnings are provided in section 2. Sparse selection methodology that leads to an explicit algorithm is discussed in section 3. Details of the numerical discretization and optimization methods employed are provided in section 4. Finally, computational examples of model discovery for ordinary (section 5.1) and partial differential equations (section 5.2) are given, demonstrating performance of the algorithm under various scenarios of noisy and incomplete data.

2 Problem formulation

Suppose that a differential equation is discretized and written in the form

$$N(u; \theta) = 0, \tag{1}$$

where $u \in \mathbb{R}^n$ is the state vector and $\theta \in \mathbb{R}^p$ encapsulates all the unknown constitutive parameters in the model, which might arise within the equation or side conditions. The function $N : \mathbb{R}^n \times \mathbb{R}^p \rightarrow \mathbb{R}^n$ is assumed to be a generic, differentiable nonlinear operator. No particular type of discretization (finite difference, finite element, neural network, etc.) is assumed at this stage, only that the approximate solution is described by the vector u .

Our main interest is to determine a sparse estimate for θ inferred from information about the solution, which could be obtained either from physical observation or derived from computation. This information is supplied in the form of noisy and possibly incomplete data $\hat{u} \in \mathbb{R}^{\hat{n}}$, which approximates u on a subset of components. This subset is denoted by D , which contains $\hat{n} \leq n$ indices, so that $\hat{u}_j \approx u_j$ for $j \in D$. The notation $v|_D$ will represent restriction to the domain of the data.

We begin with the simpler problem of estimation of θ without any regard to sparse selection. A classical approach to parameter estimation is maximum likelihood regression, which utilizes a likelihood function determined from a known (or parametric) statistical distribution of data. For example, if the

only source of uncertainty is zero-mean Gaussian noise with variance σ^2 in the data and $u^*(\theta)$ represents the exact (and unique) solution for parameters θ , the likelihood is the conditional probability

$$L(\theta) = (\sigma\sqrt{2\pi})^{-\hat{n}} \exp\left(-\frac{\|\hat{u} - u^*(\theta)\|_D\|_2^2}{2\sigma^2}\right). \quad (2)$$

Estimation of θ is therefore a nonlinear least squares fitting procedure, obtained by maximizing (2).

A more general approach takes into account uncertainty in both the data and the underlying model. For instance, $N(u; \theta)$ can be regarded as random, obeying a distribution with zero-mean and small variance. Under these assumptions, an approximate log-likelihood function can be written as [22]

$$L(\theta) = -\frac{\hat{n}}{2} \ln F(\theta), \quad F(\theta) \equiv \min_u \lambda \|\hat{u} - u\|_D\|_2^2 + \|N(u; \theta)\|_2^2. \quad (3)$$

Here λ is a ratio of variances that describes the relative uncertainty in the model compared to the data. Although λ can itself be inferred from data [22], here we regard it as a specified hyper-parameter. Expression (3) infers both parameter and solution variables θ and u in the following sense. Defining

$$\mathcal{L}_\lambda(\theta, u) = \|N(u; \theta)\|_2^2 + \lambda \|\hat{u} - u\|_D\|_2^2, \quad (4)$$

the maximum likelihood estimate is obtained by minimizing \mathcal{L}_λ over both θ and u .

Discovery of equations, as opposed to parameter estimation, must take into account a wide variety of candidate models as well as parameters. Model selection can be performed by insisting on sparsity, that is, selecting a small number of terms which provides a reasonable description of the supplied data. A typical approach is to include a sparsity promoting penalty $R(\theta)$ in the regression formulation,

$$\mathcal{L}_{\lambda, R}(\theta, u) = \|N(u; \theta)\|_2^2 + \lambda \|\hat{u} - u\|_D\|_2^2 + R(\theta). \quad (5)$$

Various choices for the penalty function are described in the next section.

3 Methodology

The problem setup described in section 2 makes no restriction on the choice of generalized model $N(u; \theta)$. For simplicity, however, we focus on the case where $N(\cdot)$ is taken to be a linear combination in the form

$$N = N_0(u) + \sum_{k=1}^p \theta_k N_k(u). \quad (6)$$

The terms $\{N_k\}$ represent a predetermined library of possible candidates, which could be specified generically, e.g. Taylor series, or derived from expert knowledge. They may also be constrained by a scientific application, for example by tailoring them to obey symmetries or underlying physics.

Given the extensive number of potential models within the candidate library, it is assumed that an optimal model contains only a few terms which are significant to describing the data. One way to suppress insignificant terms is the use of a sparsity-inducing penalty term $R(\theta)$ as in (5). A common choice for $R(\theta)$ is the direct measure of sparsity given by the l_0 "norm" of θ , which is a simple count of the number of non-zero components. Despite it being the most natural measure of sparsity, it is problematic in optimization, due to its non-smooth character, which can lead to intractably high computational complexity. Alternatives include other norms on θ , notably l_1 or l_2 . These do not exhibit the same computational difficulties associated with the l_0 penalty, but they are known to produce significant bias in parameter estimates.

In our work, we adopt a regularized l_0 penalty, leveraging a differentiable approximation [42]. This approach maintains the sparsity-promoting benefits of the l_0 measure while ensuring computational tractability through a smooth approximation. We use the specific choice

$$\|\theta\|_\epsilon = \sum_{i=1}^d \left(1 - \exp\left(-\frac{\theta_i^2}{2\epsilon^2}\right)\right), \quad (7)$$

where it is clear $\lim_{\epsilon \rightarrow 0} \|\cdot\|_{\epsilon} = \|\cdot\|_0$ (see also figure 1). For the remainder of this work, we take $R(\theta) = R\|\theta\|_{\epsilon}$, where R is a scalar hyper-parameter used to influence the degree of sparsity. This smooth approximation allows for gradient-based optimization methods, thus enabling more practical implementations in high-dimensional settings.

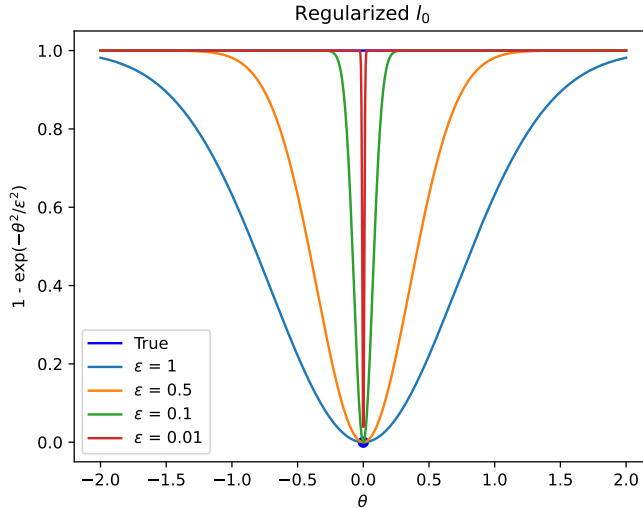


Figure 1: Visualization of regularized l_0 penalty compared to the true l_0 penalty under different values of ϵ .

Observe that minimization of (5) using the regularized l_0 penalty does not immediately lead to a sparse parameter set, as it is unlikely that the components of the minimizer θ will be identically zero. The regularized sparsity penalty can, on the other hand, be useful to identify terms which have little relevance. This allows us to identify good sparse models which can be compared using criteria explained in section 3.1. This will lead to a complete discovery algorithm discussed in section 3.2.

3.1 Model comparison and subset selection

Under assumptions of model sparsity, it is necessary to leverage methods for selecting and comparing different subsets of model terms. The most straightforward methods for selecting new subsets utilize a predefined threshold value, excluding model terms with parameters below this limit (e.g. [12, 53]). A similar approach is to remove a specified number of terms corresponding to the lowest parameter values. In our testing, the latter method resulted in a higher number of candidates tested but tended to produce more satisfactory results. When working within this framework, the user may need to evaluate their computational bandwidth to decide which one is best. For the sake of simplicity, we choose to drop a predefined number of model terms each iteration, with possible backtracking discussed in the next section.

The likelihood function (4) alone is insufficient to competitively test models. Indeed, the minimum of this function will only increase as smaller and smaller subsets of potential models are considered. To address this, we use an information-theoretic approach to balance the predictive power of a model with its complexity, as defined by the number of terms in the model. Two possible statistical measures are the Akaike Information Criteria (AIC) [2] and the Bayesian information criteria (BIC) [56]. In our experience, BIC tended to result in better performance due to its higher penalization of excess parameters, and was chosen as the preferred method throughout this work.

The Bayesian Information Criterion (BIC), also known as the Schwarz criterion, is a widely used model selection tool used in statistical analysis and machine learning. It seeks to balance the goodness of fit of the model with its complexity, similarly to AIC, but places a higher penalty on models with

more parameters, making it more stringent against overfitting in scenarios with large datasets. The BIC is defined as:

$$\text{BIC} = \ln(n)d - 2 \log L, \quad (8)$$

where d is the number of parameters in the model and L is the likelihood of the model given the data. This formulation shows the BIC’s increasing penalty on complexity through the $\ln(n)$ term, which grows with the size of the data set. Plugging our log-likelihood function given by equation (3) into the BIC formulation, we use the final form,

$$\text{BIC}(u, d) = \ln(\hat{n})d + \hat{n} \ln \left(\|N(u; \theta)\|_2^2 + \lambda \|\hat{u} - u\|_D\|_2^2 \right). \quad (9)$$

When comparing two competing models, the best has the lower BIC score.

3.2 Model selection algorithm

Given a library with p potential terms, there are 2^p subset models, so it is impractical to consider the entire set of sparse models. Instead our aim is to efficiently select and assess a limited range of possibilities, effectively sampling near the so-called “Pareto Front” associated with the simultaneous objectives of high model accuracy and low complexity. The method for achieving this is outlined as follows.

Our method begins with simultaneous minimization on the non-sparse loss \mathcal{L}_λ and the sparse loss $\mathcal{L}_{\lambda,R}$. The first pair of optimizations uses provided initial guesses u_0, θ_0 , and thereafter uses the results of previous optimizations. The dual loss functions serve distinct purposes: \mathcal{L}_λ informs us about the likelihood of a model given a specific set of parameters, while $\mathcal{L}_{\lambda,R}$ encourages irrelevant terms to be small, aiding in the selection of new subsets to test. The results of optimizing at step i are defined as

$$(\theta_{\lambda_i}, u_{\lambda_i}) = \arg \min_{\theta, u} \mathcal{L}_\lambda(u, \theta \odot M_i) \quad (10)$$

$$(\theta_{R_i}, u_{R_i}) = \arg \min_{\theta, u} \mathcal{L}_{\lambda,R}(u, \theta \odot M_i) \quad (11)$$

In these expressions, $M_i \in \{0, 1\}^p$ represents a mask for the i -th parameter subset, determining which terms are under consideration in the optimization, and \odot represents the element-wise Hadamard product. The solution from equation (10), $(\theta_{\lambda_i}, u_{\lambda_i})$, is used to quantify the models likelihood and compare its performance against previously tested models using the Bayesian information criterion (BIC) as detailed in section 3.1. Initially, any proposed model is accepted to establish a baseline for comparison. In subsequent iterations, if a model produces a BIC score lower than the best score tested so far, it is set as the new best model and prompts the selection of another subset for testing. Specifically, we adjust the mask to exclude a user defined k smallest parameters of θ_{R_i} which have not been removed previously. This simplifies to setting k terms in the proposed mask M_{i+1} to zero where the current mask components M_i are one, ensuring parameters dropped in earlier iterations are not reconsidered.

The algorithm adaptively refines the search when a new candidate model does not have a smaller information criteria score. Upon the first model rejection, the procedure reverts to the previously accepted parameters and narrows the search by reducing the number of parameters dropped in each iteration to one. This strategy hones in on the current best solution by incrementally removing one model term at a time until it encounters another rejection. If the removal of a single parameter leads to an accepted model, it is assumed that no further backward adjustments are necessary. Conversely, if this minimal adjustment is rejected outright, the algorithm reverts to the best-performing model and starts reintroducing previously removed terms, one at a time. To facilitate this process, the algorithm keeps a record of the second-best model, aiding in the identification and reintroduction of the largest parameter absent in the current best model.

This approach is designed not only to identify the most parsimonious model but also to methodically explore and document the performance of various models. Each tested model, along with its corresponding information criterion (IC) scores, is recorded, allowing for a comprehensive review by experts. The full procedure is outlined in algorithm 1 and figure 2 illustrates how the algorithm dynamically navigates through the model space by alternating between advancing forward with new model

configurations and stepping back to refine prior selections. This strategy ensures that the search space is efficiently explored, increasing the likelihood of identifying the most effective model configuration.

Algorithm 1 Parallel Subset Selection with Sparsity

```

1: Inputs:
2: %  $u_0 \in \mathbb{R}^n$ : Initial state vector,  $\theta_0 \in \mathbb{R}^p$ : Initial parameters,  $k_0$ : Parameter drop count per iteration
3: %  $\lambda$ : Regularization for data fit,  $R$ : Regularization for sparse sparse penalty.
4: procedure OPTIMIZEMODELS( $u_0, \theta_0, k_0, \lambda, R$ )
5:    $bestIC \leftarrow \infty, k \leftarrow k_0, i \leftarrow 0, Forward \leftarrow True$ 
6:   while  $k \neq 0$  do
7:     Execute in parallel:
8:      $(\theta_{\lambda_i}, u_{\lambda_i}) \leftarrow \arg \min_{\theta, u} \mathcal{L}_{\lambda}(u, \theta \cdot M_i)$  ▷ Optimize non-sparse model
9:      $(\theta_{R_i}, u_{R_i}) \leftarrow \arg \min_{\theta, u} \mathcal{L}_{\lambda, R}(u, \theta \cdot M_i)$  ▷ Optimize sparse model
10:    if  $IC(u_{\lambda_i}, nnz(M_i)) < bestIC$  then
11:       $bestIC \leftarrow IC(u_{\lambda_i}, nnz(M_i))$ 
12:       $(\theta^*, u^*) \leftarrow (\theta_{\lambda_i}, u_{\lambda_i})$ 
13:      if  $Forward$  then
14:         $M_{i+1} \leftarrow 0$  for  $k$  smallest  $|\theta_{R_i}|$  where  $M_i = 1$  ▷ Advance model reduction
15:      else
16:         $k \leftarrow k - 1$ 
17:         $M_{i+1} \leftarrow 0$  for  $k$  smallest  $|\theta_A|$  where  $M_A = 1$  ▷ Add terms in
18:      end if
19:      else if  $k \neq 1$  then
20:         $\theta_A, M_A \leftarrow \theta_{R_{i-2}}, M_{i-2}$  ▷ Store second best model
21:         $k \leftarrow 1$ 
22:         $M_{i+1} \leftarrow 0$  for  $k$  smallest  $|\theta_{R_{i-1}}|$  where  $M_{i-1} = 1$  ▷ Refine around last accepted
23:      else if  $Forward$  then
24:         $Forward \leftarrow False$  ▷ Turn backwards mode on
25:         $k \leftarrow k_0 - 1$ 
26:         $M_{i+1} \leftarrow 0$  for  $k$  smallest  $|\theta_A|$  where  $M_A = 1$  ▷ Begin backward adjustments from best model
27:      else
28:         $k \leftarrow 0$  ▷ End iterations
29:      end if
30:       $i \leftarrow i + 1$ 
31:    end while
32:    return  $(\theta^*, u^*)$  ▷ Return the best state and parameters
33: end procedure

```

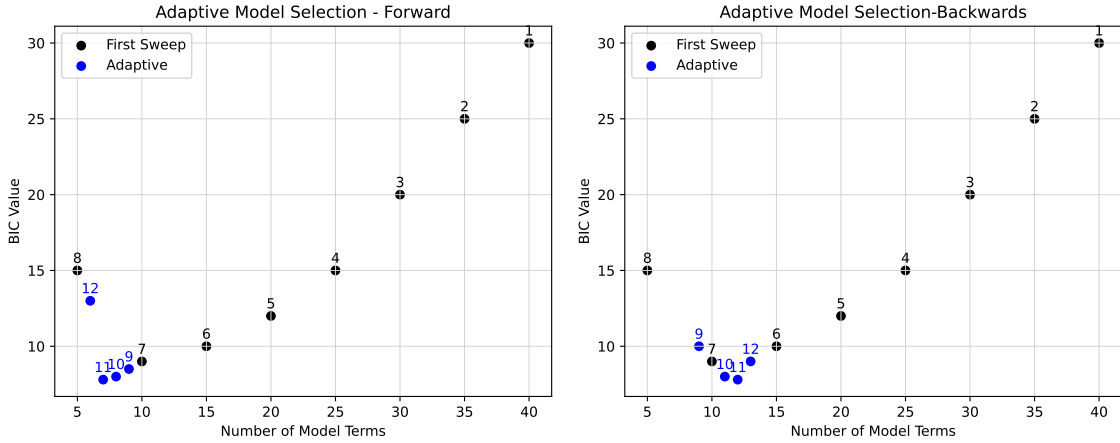


Figure 2: Visualization of algorithm 1’s methodology to hone in on the correct terms under two different scenarios with parameter drop count $k = 5$. Iteration numbers are shown above each point, while both cases show the first model is rejected in iteration 8. Left shows acceptance of small forward steps resulting in no need to go to more complex models. Right shows a small forward step is rejected, resulting in the need for backward steps or testing more complex models.

3.3 Implementation

The loss function $\mathcal{L}_{\lambda,R}(\theta, u)$ in discrete form is computed as:

$$\mathcal{L}_{\lambda,R}(\theta, u) = \underbrace{\frac{1}{n} \sum_{i=1}^n N(u_i; \theta)^2}_{\text{Model Error}} + \underbrace{\frac{\lambda}{\hat{n}} \sum_{i \in D} (\hat{u}_i - u_i)^2}_{\text{Data Error}} + \underbrace{\frac{R}{d} \sum_{i=1}^d \left(1 - \exp\left(-\frac{\theta_i^2}{2\epsilon^2}\right) \right)}_{\text{Sparse Penalty}}. \quad (12)$$

where D is the set of indices in the domain at which data is available. It follows $\mathcal{L}_{\lambda}(\theta, u)$ requires the same implementation with the exclusion of the sparsity-inducing term. While the data error and sparse penalty terms are rather straightforward to compute, there are many choices when it comes to discretizing the model. In this work we are concerned with differential equations formulated as the linear combination shown in equation (6), and the specific choice of first order time derivatives defined by the choice $N_0(u) \equiv \frac{d}{dt}u$. Time derivatives are computed by the semi-implicit trapezoidal rule, which offers a good balance between accuracy and algorithm complexity. The discretization formula is given by

$$N(u_i; \theta) = \frac{u_{i,t+1} - u_{i,t}}{\Delta t} - \sum_{k=1}^p \theta_k N_k \left(\frac{u_{i,t+1} + u_{i,t}}{2} \right), \quad (13)$$

where $u_{i,t}$ and $u_{i,t+1}$ represent the values of u at spatial points i and times t and $t + 1$, respectively, and Δt is the time step. The functions $\{N_k\}$ are model terms of a predefined library, parameterized by $\{\theta_k\}$.

The implementation of ODEs and PDEs does not differ in the setup, rather only in the choice of library functions. Prior to discretization, when dealing with ODEs, each component of the state vector u represents a dynamic variable, such as $\{x_1, x_2, \dots, x_n\}$. The model library might look like

$$N = \begin{bmatrix} \dot{x}_1 \\ \dot{x}_2 \\ \vdots \\ \dot{x}_n \end{bmatrix} - \begin{bmatrix} x_1 & x_2 & x_1 x_2 & x_1 x_n & \cdots \\ x_1 & x_2 & x_1 x_2 & x_1 x_n & \cdots \\ \vdots & \vdots & \vdots & \vdots & \\ x_1 & x_2 & x_1 x_2 & x_1 x_n & \cdots \end{bmatrix} \circ \theta, \quad (14)$$

where $M \circ \theta$ denotes the Hadamard product of a matrix M and parameter matrix θ , followed by summation over rows.

For PDEs, the inclusion of spatial derivatives introduces additional complexity. In this work the spatial derivatives are computed with second-order centered finite-difference stencils due to their balance between accuracy and computational efficiency. We note if the boundary conditions are known, they may seamlessly be included in this framework. For the results presented, we assumed that we had no knowledge of the boundary conditions and instead optimize over the interior of the domain. In this case, the model library might look like

$$N = u_t - \left[u \quad \frac{\partial u}{\partial x} \quad \frac{\partial^2 u}{\partial x^2} \quad u^2 \quad \cdots \right] \circ \theta. \quad (15)$$

where u_t represents the time derivative of u and $\frac{\partial u}{\partial x}$ and $\frac{\partial^2 u}{\partial x^2}$ represent the first and second spatial derivatives of u , respectively.

4 Optimization

Minimization of the loss functions described in equations (4) and (5) presents a challenging high-dimensional and potentially non-convex optimization landscape. First-order gradient descent methods popular in machine learning such as Adam [30], were initially investigated for our situation. Despite the speed of each iteration, these methods require an excessive number of iterations to converge or fail to find the

correct solution altogether. This is unsurprising, as the mathematical structure of gradient descent here is similar to numerical solutions of high-order parabolic equations, where time-implicit methods are generally used. This necessitates a shift to second-order optimization methods, where some common algorithms are Levenberg-Marquardt (LM) [33, 39], nonlinear conjugate gradient [17], trust region newton conjugate gradient (trust-ncg)[58], and the limited-memory Broyden–Fletcher–Goldfarb–Shanno (L-BFGS) [35]. We tested all of these methods for our problems and found that a variant of the original Levenberg-Marquardt method proved to be the most robust, and is used in the computational examples in section 5.

Developed for nonlinear least-squares problems, the original LM algorithm approximates the Hessian using a product of Jacobian matrices. It has since been generalized for scalar-valued functions using the true Hessian [44]. Often categorized as a second-order trust-region method, the LM algorithm approaches the optimization by solving a sequence of linearized problems, where it combines the principles of Newton’s method and gradient descent. This is achieved by scaling the diagonal of the Hessian matrix to blend these methods effectively. The precise details used in this paper are given in algorithm 2.

The main computational effort for this form of the LM algorithm involves constructing the Hessian $H(x)$ and solving $H_\alpha d_k = -g$, where $H_\alpha = H + \alpha \text{diag}(H)$ is the modified Hessian and g is the gradient. The parameter α is adjusted adaptively to ensure that a local minimum is found. In the proposed framework, the true Hessian is very sparse, allowing for efficient construction, detailed in Section 4.1. The time complexity is therefore dominated by the linear algebra. In this work, the linear solve for d_k uses sparse Cholesky factorization on small to medium-sized problems, whereas the conjugate gradient (CG) method is used for large problems where matrix factorization is infeasible.

Algorithm 2 Levenberg-Marquardt Optimization

```

1: procedure LEVENBERGMARQUARDT( $f, \mathbf{x}, \alpha, \tau, \epsilon$ )
2:   Initialize  $\alpha, \tau_1, \tau_2$  (e.g.,  $\alpha = 1.0, \tau_1, \tau_2 \in (1, 10)$ )
3:   while not converged do
4:      $H \leftarrow \frac{\partial^2 f}{\partial \mathbf{x}^2}$  ▷ Compute Hessian
5:      $H_\alpha \leftarrow H + \alpha \cdot \text{diag}(H)$  ▷ Scale Hessian diagonal
6:      $g \leftarrow \frac{\partial f}{\partial \mathbf{x}}$  ▷ Compute gradient
7:     Solve  $H_\alpha d_k = -g$  for  $d_k$ 
8:     if  $f(\mathbf{x} + d_k) < f(\mathbf{x})$  then
9:        $\mathbf{x} \leftarrow \mathbf{x} + d_k$  ▷ Update parameters
10:       $\alpha \leftarrow \alpha / \tau_1$  ▷ Towards Newton Step
11:     else
12:        $\alpha \leftarrow \alpha \cdot \tau_2$  ▷ Towards Gradient Descent
13:     end if
14:   end while
15:   return  $\mathbf{x}$ 
16: end procedure

```

4.1 Exploiting sparsity

In higher-order optimization, efficiently computing the Hessian matrix is a fundamental challenge. Our approach benefits from a sparse Hessian that stems from the model discretization, and enhances the feasibility of employing advanced optimization techniques. A key aspect of our model is its compatibility with automatic differentiation, which simplifies construction of the Hessian across various scenarios. To effectively integrate sparsity and automatic differentiation, we first identify the sparsity structure of the Hessian, and subsequently apply graph coloring techniques to minimize the number of Hessian-vector products (HVPs) needed to compute the entire sparse Hessian.

4.1.1 Computing the Hessian structure

To identify the sparsity pattern of the Hessian, we analyze the loss function in its discrete form given by equation (12). Considering each of the three components as independent functions, it is clear the data

error and sparse penalty terms have no dependence on neighbor interactions, resulting in a contribution to the Hessian matrix only along the diagonal. Derivatives of the form

$$\frac{\partial^2 \|N(u; \theta)\|_2^2}{\partial u_m \partial \theta_n} \quad (16)$$

are generally all non-zero, which creates a dense but small portion of the Hessian that is computed directly.

The largest portion of the Hessian corresponds to state derivatives,

$$\frac{\partial^2 \|N(u; \theta)\|_2^2}{\partial u_m \partial u_n} = \sum_{i,j \in N(m) \cap N(n)} \frac{\partial^2 N(u_i; \theta)^2}{\partial u_i \partial u_j}. \quad (17)$$

where $N(x)$ denotes the neighbors connected at the x^{th} grid point. This relationship is provided by the finite difference stencils, which are known in advance and only computed once. The neighbor relation can also be associated with a graph with vertices labelled $1, 2, \dots, n$ with edges of the form $(i, N(i))$. The sparse contributions in (17) can be efficiently computed using graph coloring techniques, as explained next.

4.1.2 Graph coloring and Hessian vector product

The Hessian-vector product of a function f and vector v , is

$$Hv = \nabla^2 f(x)v = \nabla[\nabla f(x) \cdot v] \equiv \nabla g(x)$$

where $v \in \mathbb{R}^n$ is a vector and $g : \mathbb{R}^n \rightarrow \mathbb{R}$. Computing this involves automatic differentiation to find the gradient of the scalar function g , rather than directly computing the Hessian of f . The computational complexity in calculating a dense Hessian is comparable to computing the HVP over all n coordinate vectors. On the other hand, for sparse matrices, we need to obtain only a small set of binary vectors d_1, d_2, \dots, d_k , such that Hd_1, Hd_2, \dots, Hd_k determine H entirely. This problem can be reformulated as a graph coloring problem, and particularly for symmetric matrices, a star coloring problem [20]. Star coloring is a graph coloring approach where adjacent vertices have distinct colors, and every path of length three within the graph uses at least three distinct colors. This problem determines a minimal set of binary vectors, each corresponding to one color, so that the HVP Hd_j has non-zero components corresponding to a subset of Hessian matrix entries. Star coloring is an NP-hard problem, so we instead utilize an approximate star coloring algorithm [14, 45] which has nearly optimal performance.

5 Results

This section presents numerical examples to illustrate the proposed method's efficacy in handling ordinary and partial differential equations under various conditions of noise and missing data. The discretization was performed on a uniform grid, though this is not a strict requirement of the method. Non-uniform data, for example, could also be accommodated by a combination of interpolation and restriction to a smaller domain. We introduce normally distributed noise into our simulation data as follows:

$$u_{\text{noise}} = u^* + \mathcal{N}(0, \sigma^2), \quad \sigma = (\% \text{ noise}) \times \text{standard deviation of } u^*,$$

where u^* denotes clean data from direct simulation. To facilitate the fitting process, the initial guess for the model states is derived from the available data, with missing entries filled using a forward fill method based on the next available non-missing value. This method provides a practical starting point for the optimization process and helps refine the estimates for the missing data points. We examine the effectiveness of our approach across various levels of data availability and noise intensity. All data and codes used in this manuscript are publicly available on GitHub at <https://github.com/TeddyMeissner/DEDi>.

5.1 Ordinary differential equations

5.1.1 Van der Pol Oscillator

The Van der Pol system

$$\begin{aligned}\dot{x} &= y, \\ \dot{y} &= \mu(1 - x^2)y - x,\end{aligned}\tag{18}$$

initially formulated to model electrical circuits with vacuum tubes, is a non-conservative oscillator with non-linear damping. It is widely used in system identification and nonlinear dynamics studies, offering a classic example of a model exhibiting limit cycle behavior and self-sustained oscillations.

To generate data, we used the parameter $\mu = 2$ and initial condition $(x_0, y_0) = (0, 2)$. The simulations were performed with the explicit Runge-Kutta method of order 5(4) (RK45), over the interval $t \in (0, 10)$ with a step size of $dt = 0.02$, resulting in a total of 1002 data points across 501 time steps. The initial library provided was:

$$N = \begin{bmatrix} \dot{x}_1 \\ \dot{x}_2 \end{bmatrix} - \begin{bmatrix} x_1 & x_2 & x_1x_2 & x_1^2 & x_2^2 & x_1^2x_2 & x_1x_2^2 & x_1^3 & x_2^3 \\ x_1 & x_2 & x_1x_2 & x_1^2 & x_2^2 & x_1^2x_2 & x_1x_2^2 & x_1^3 & x_2^3 \end{bmatrix} \circ \theta,$$

where θ is a 2×9 matrix of coefficients.

All test cases shown were generated with hyper-parameters $(\lambda, R) = (10^{-2}, 10^{-4})$. The effectiveness of our method is highlighted in Figure 3, where the reconstructed states align closely with the true states, greatly outperforming the raw data. This demonstrates that our approach not only identifies the underlying model accurately but also acts as a nonlinear filter, improving data quality in a manner similar to data assimilation techniques. Table 1 presents the results from various test scenarios, indicating that the method performs well even in high noise and significant data loss conditions.

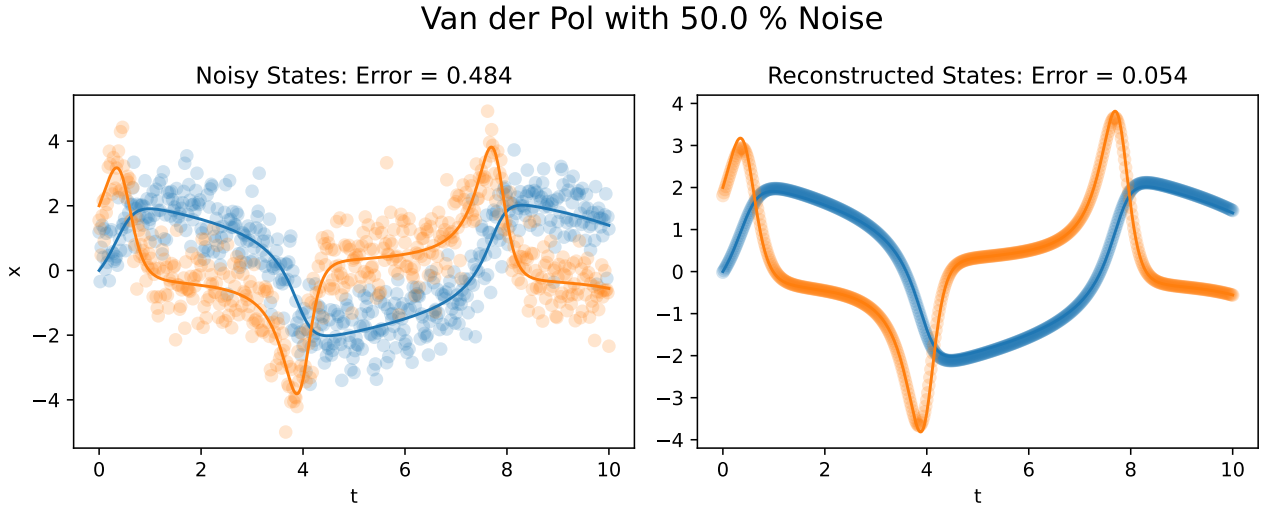


Figure 3: Visualization of the Van der Pol oscillator components over time. The continuous line depicts the true states of the system, while the scatter dots indicate observed data points in the left image and reconstructed states in the right image. Above the plot, the relative error between the noisy and reconstructed states compared to the true states is illustrated.

Noise	Missing Data	Missing Terms	Extra Terms	Model Discovered
30%	20%	0	0	$\dot{x}_1 = 1.026x_2$ $\dot{x}_2 = -0.949x_1 + 1.878x_2 - 1.758x_1^2x_2$
50%	20%	0	0	$\dot{x}_1 = 1.043x_2$ $\dot{x}_2 = -0.918x_1 + 1.801x_2 - 1.614x_1^2x_2$
70%	20%	0	0	$\dot{x}_1 = 1.059x_2$ $\dot{x}_2 = -0.889x_1 + 1.726x_2 - 1.482x_1^2x_2$
30%	40%	0	0	$\dot{x}_1 = 1.029x_2$ $\dot{x}_2 = -0.954x_1 + 1.946x_2 - 1.879x_1^2x_2$
50%	40%	1	1	$\dot{x}_1 = 1.062x_2$ $\dot{x}_2 = 2.172x_2 - 1.729x_1^2x_2 - 0.301x_1^3$
70%	40%	1	7	$\dot{x}_1 = -0.646x_1 + 116.189x_2 + 36.376x_1x_2^2 - 32.721x_1^2x_2 - 20.329x_2^3$ $\dot{x}_2 = -46.483x_1 - 52.753x_2 - 9.025x_1x_2^2 + 12.695x_1^3 + 9.577x_2^3$

Table 1: Summary of regression results for different levels of noise and missing data in the Van der Pol Oscillator.

5.1.2 The Lorenz system

The Lorenz equations [37]

$$\begin{aligned}
 \dot{x} &= \sigma(y - x) \\
 \dot{y} &= x(\rho - z) + y \\
 \dot{z} &= xy - \beta y
 \end{aligned} \tag{19}$$

were originally derived from models of atmospheric convection, and have become the standard example of chaotic behavior in ordinary differential equations. They have also emerged as a canonical test case in studies of system identification due to their deterministic yet complex behavior.

We generated data using the parameters $(\sigma, \rho, \beta) = (10, 28, 8/3)$ and initial conditions $(x_0, y_0, z_0) = (-8, 8, 27)$. The simulations were performed with RK45 over the interval $t \in (0, 5)$ with a step size of $dt = 0.02$, resulting in a total of 753 data points across 251 time steps. The initial library provided was

$$N = \begin{bmatrix} \dot{x}_1 \\ \dot{x}_2 \\ \dot{x}_3 \end{bmatrix} - \begin{bmatrix} x_1 & x_2 & x_3 & x_1x_2 & x_1x_3 & x_2x_3 & x_1^2 & x_2^2 & x_3^2 \\ x_1 & x_2 & x_3 & x_1x_2 & x_1x_3 & x_2x_3 & x_1^2 & x_2^2 & x_3^2 \\ x_1 & x_2 & x_3 & x_1x_2 & x_1x_3 & x_2x_3 & x_1^2 & x_2^2 & x_3^2 \end{bmatrix} \odot \theta,$$

where θ is a 3×9 matrix of coefficients.

All test cases shown were generated with hyper-parameters $(\lambda, R) = (10^{-2}, 10^{-4})$. Similar to the Van der Pol example, Figure 4 shows the ability of our method to reconstruct states which align closely with the true states, even with very noisy observations. Table 2 presents the results from various test scenarios, which exhibits similar success to the previous example and was able to determine reasonable models even in high noise and significant data loss conditions.

Lorenz with 50.0 % Noise

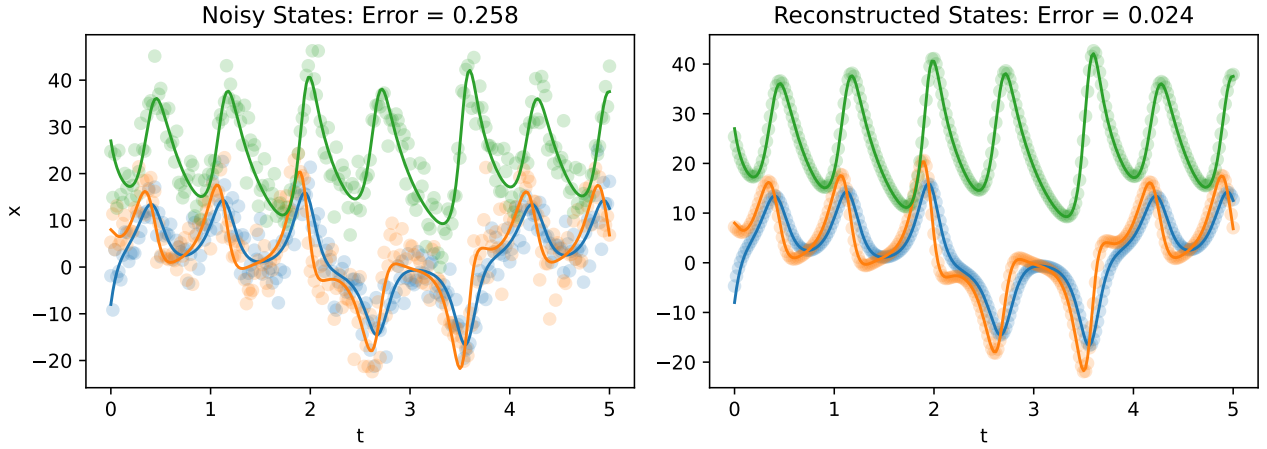


Figure 4: Visualization of the Lorenz system’s components over time. The continuous line represents the true states of the system. In the left image, scatter dots show observed data points, while in the right image, they depict reconstructed states. Above the plot, the relative error between the noisy and reconstructed states compared to the true states is illustrated.

Noise	Missing Data	Missing Terms	Extra Terms	Model Discovered
30%	20%	0	0	$\dot{x}_1 = -9.622x_1 + 9.568x_2$ $\dot{x}_2 = 29.314x_1 - 1.215x_2 - 1.030x_1x_3$ $\dot{x}_3 = -2.677x_3 + 1.029x_1x_2$
50%	20%	0	0	$\dot{x}_1 = -9.370x_1 + 9.274x_2$ $\dot{x}_2 = 30.132x_1 - 1.335x_2 - 1.048x_1x_3$ $\dot{x}_3 = -2.681x_3 + 1.044x_1x_2$
70%	20%	1	2	$\dot{x}_1 = -8.943x_1 + 8.700x_2$ $\dot{x}_2 = 28.658x_1 - 0.984x_2 - 1.006x_1x_3$ $\dot{x}_3 = -3.210x_3 + 0.557x_1^2 + 0.518x_2^2$
30%	40%	0	0	$\dot{x}_1 = -9.409x_1 + 9.389x_2$ $\dot{x}_2 = 29.767x_1 - 1.300x_2 - 1.046x_1x_3$ $\dot{x}_3 = -2.660x_3 + 1.035x_1x_2$
50%	40%	0	0	$\dot{x}_1 = -9.074x_1 + 9.044x_2$ $\dot{x}_2 = 30.767x_1 - 1.456x_2 - 1.071x_1x_3$ $\dot{x}_3 = -2.654x_3 + 1.056x_1x_2$
70%	40%	1	10	$\dot{x}_1 = -0.328x_1 + 7.046x_2 + 0.588x_1x_2 - 0.265x_1x_3 - 0.728x_1^2$ $\dot{x}_2 = 21.642x_1 + 2.427x_2 + 0.273x_3 + 1.656x_1x_2 - 1.071x_1x_3 - 1.065x_2^2$ $\dot{x}_3 = 1.393x_1 - 0.583x_2 - 3.195x_3 + 0.667x_1^2 + 0.474x_2^2$

Table 2: Summary of regression results for different levels of noise and missing data in the Lorenz system.

5.2 Partial differential equations

5.2.1 Kuramoto-Sivashinsky

The Kuramoto-Sivashinsky (KS) equation [32] is a fundamental nonlinear partial differential equation that exhibits chaotic behavior under certain conditions. It is used to model various physical phenomena, including diffusive instabilities in laminar flame fronts, reaction-diffusion systems, and the flow of

liquid films. The equation in one spatial dimension is given by:

$$u_t = auu_x + bu_{xx} + cu_{xxx}, \quad (20)$$

where $u(x, t)$ represents the scalar field of interest, x is the spatial coordinate, and t is time. The equation combines nonlinear advection and linear instabilities, which together lead to complex dynamical behavior, including chaos and pattern formation. For this example we generated data using the parameters $(a, b, c) = (1, -1, -1)$ and initial data $u(x, 0) = -2 \sin(12\pi x/L) + 2 \exp(-(x-2)^2/5)$. Periodic boundary conditions were used to generate the solution, although our algorithm does not assume this.

The simulations were performed with spectral differentiation in space and trapezoidal rule for time integration. The solution presented, $u(x, t) : [0, L] \times [0, T] \rightarrow \mathbb{R}$, was sampled with $T = 38.4$, $L = 40$ and $dt = 0.3$, $dx = .3125$. The result is 128 spatial grid points for 128 times or 16,384 total data points. The library used was

$$N = u_t - [u \quad u^2 \quad u^3 \quad u_x \quad u_{xx} \quad u_{xxx} \quad u_{xxxx} \quad uu_x \quad u^2u_x] \theta, \quad (21)$$

where θ is a column vector of coefficients.

All test cases shown were generated with hyper-parameters $(\lambda, R) = (10^{-2}, 10^{-4})$. This method demonstrated remarkable success in identifying the correct underlying equations despite significant noise and numerous missing data points, as evidenced in Table 3. Additionally, Figure 5 illustrates the method's capability to reconstruct the data. It is important to note the optimization is done without any assumptions on boundary conditions, which accounts for the increased error observed near the boundaries.

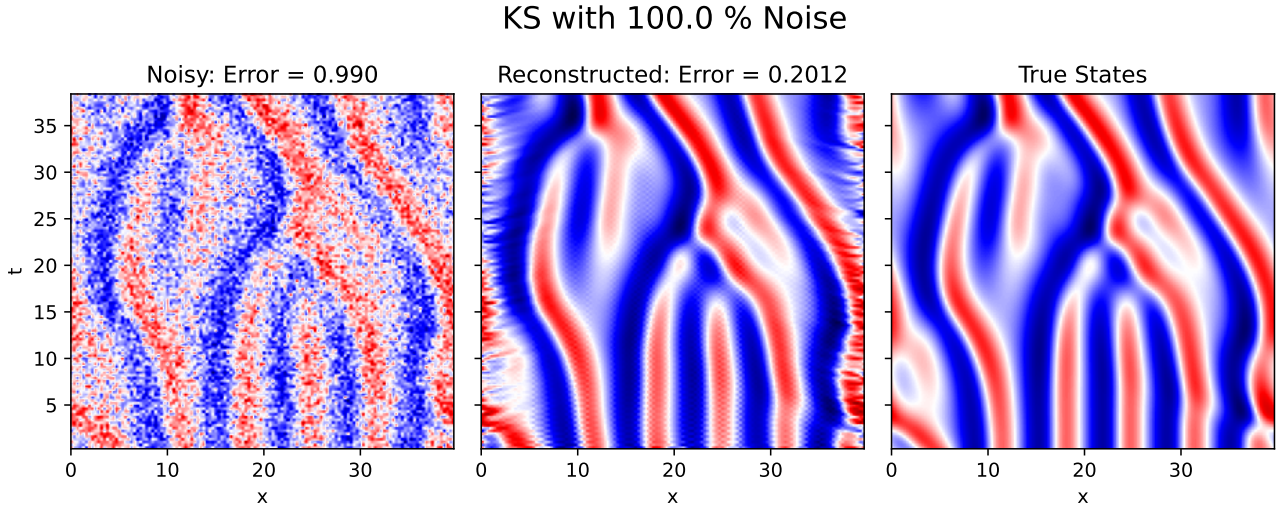


Figure 5: Left: Data with 100% normal noise added. Middle: Reconstructed states found from optimization procedure. Right: Clean data from numerical simulation.

Noise	Missing Data	Missing Terms	Extra Terms	Model Discovered
30%	40%	0	0	$u_t = -1.007u_{xx} - 1.020u_{xxxx} + 1.019uu_x$
50%	40%	0	0	$u_t = -1.008u_{xx} - 1.022u_{xxxx} + 1.017uu_x$
100%	40%	0	0	$u_t = -1.012u_{xx} - 1.027u_{xxxx} + 1.008uu_x$
30%	60%	0	0	$u_t = -1.004u_{xx} - 1.015u_{xxxx} + 1.020uu_x$
50%	60%	0	0	$u_t = -1.003u_{xx} - 1.013u_{xxxx} + 1.017uu_x$
100%	60%	1	4	$u_t = -0.075u_{xxxx} + 0.373uu_x + 0.035u^3 - 0.595u_x + 0.366u_{xxx} + 0.839u^2u_x$

Table 3: Summary of regression results for different levels of noise and missing data in the KS equation.

5.2.2 Allen-Cahn 2D

The Allen-Cahn (AC) equation [3] is a widely studied nonlinear partial differential equation that describes the process of phase separation in multi-component alloy systems, among other phenomena. It is particularly known for its application in modeling the evolution of interfaces between different phases. In two dimensions, the equation captures dynamics of phase boundary curves in a plane. The equation is given by

$$u_t = \Delta u + u - u^3, \quad (22)$$

where $\Delta u := u_{xx} + u_{yy}$ and $u(x, y, t)$ denotes the order parameter that distinguishes between the different phases, x and y are the spatial coordinates in the 2D domain. Whereas the simulations utilize Neumann boundary conditions, the discovery algorithm does not need or assume this.

In this example we explore the possibility of discovering the governing equations from only two time steps. In effect, we are learning the phase boundary dynamics by virtue of having enough spatially distributed data. The AC equation is simulated using a numerical method that incorporates iterative convexity splitting with a linear extrapolation predictor [23]. The simulation is performed on a two-dimensional uniform spatial domain discretized into a grid of size $N \times N$, where $N = 256$ and $dx = 40/127$. The initial condition for the simulation is a slightly asymmetric phase fraction,

$$u(x, y, 0) = 0.1(\text{rand}(N, N) - 0.5)$$

where $\text{rand}(N, N)$ generates a uniform random distribution between 0 and 1 across the grid. The time integration is performed using a time step $dt = 1 \times 10^{-2}$. Data points are *only* captured at two specific times, $t = 25$ and $t = 26$ seconds, to analyze the evolution of the phase field at these moments. The library used was,

$$N = u_t - [u \quad u^3 \quad u_x \quad u_y \quad u_{xx} \quad u_{yy} \quad uu_x \quad uu_y \quad u^2u_x \quad u^2u_y] \theta. \quad (23)$$

All test cases shown were generated with hyper-parameters $(\lambda, R) = (10^{-2}, 10^{-6})$. Remarkably, our methodology successfully identified the governing equations from only two time steps, demonstrating its capabilities in extreme circumstances. This result shows the power of introducing state variables dynamically related to the parameters. Table 4 illustrates the method's robust performance under moderate noise and missing data. However, it is important to note that extending this approach beyond the demonstrated conditions is challenging for two main reasons: the limited temporal data restricts model depth, and escalating data sizes intensify the optimization demands. Therefore, the conjugate gradient (CG) method, pivotal for the linear algebra step in LM optimization, often requires an effective preconditioner, which remained elusive in our tests. Further discussion on the necessity of preconditioners for scaling this model to larger data sets is detailed in Section 6.

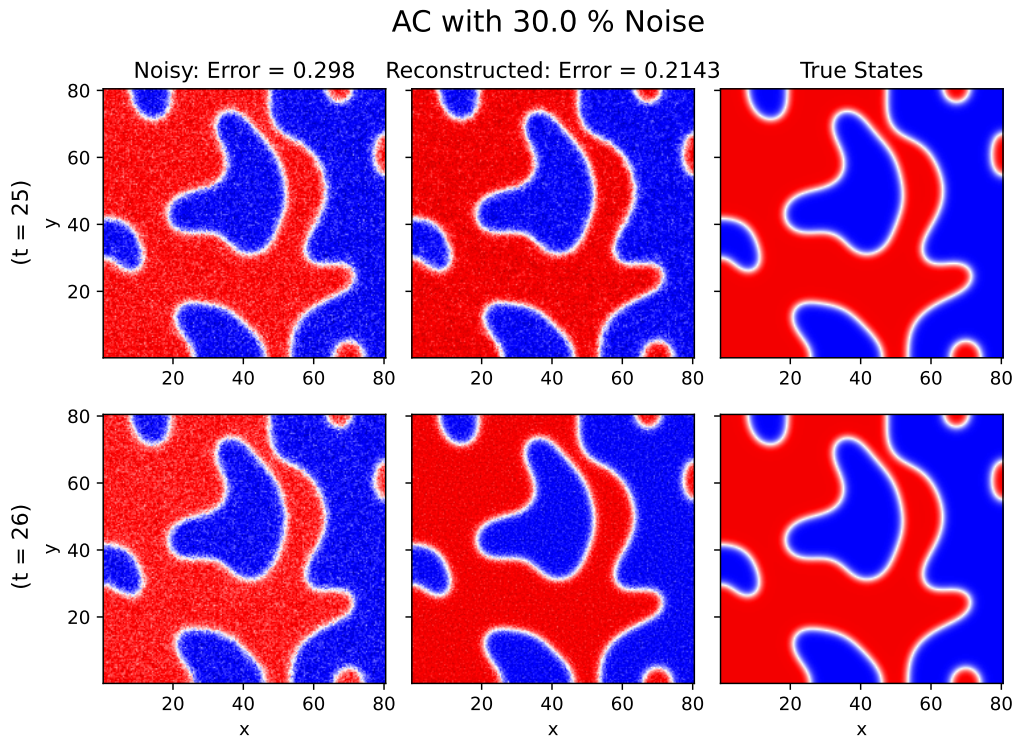


Figure 6: Top row shows AC solution for time $t = 25$, bottom row shows $t = 26$. Left: Data with 30% normal noise added. Middle: Reconstructed states found from optimization procedure. Right: Clean data from numerical simulation.

Noise	Missing Data	Missing Terms	Extra Terms	Model Discovered
10%	0%	0	0	$u_t = 0.974u_{xx} + 0.985u_{yy} + 0.972u - 0.973u^3$
20%	0%	0	0	$u_t = 0.929u_{xx} + 0.952u_{yy} + 0.939u - 0.940u^3$
30%	0%	0	0	$u_t = 0.864u_{xx} + 0.904u_{yy} + 0.889u - 0.889u^3$
10%	10%	0	0	$u_t = 0.959u_{xx} + 0.957u_{yy} + 0.949u - 0.949u^3$

Table 4: Summary of regression results for different levels of noise and missing data in the AC equation.

6 Discussion and conclusions

In this study, we introduced a novel framework for model discovery that is robust in extreme situations of limited data and substantial noise. Our approach excels in inferring states and parameters simultaneously, achieving high accuracy without relying on global or network function approximations for state variables, or attempting to differentiate noisy data. Additionally, local discretization schemes can be implemented that both allow for arbitrary accuracy of solution representations and facilitate the use of second-order optimization techniques by yielding a sparse Hessian.

Our approach was chosen to limit the requirement for significant user configuration and manual fine tuning. This is often a disadvantage of many data-driven algorithms where there is a need to supply numerous hyper-parameters, neural architectures, or preprocess or filter data. Although the algorithmic parameters λ and R were fixed in our examples, there are a number of methods that can automate selection of these. The loss function (4) is related to Tikonov Regularization [61, 62], where under known noise ξ , one may adapt λ such that $\xi \approx \lambda \|\hat{u} - u|_D\|_2^2$, often referred to as the Morozov discrepancy principle [43]. Alternatively, when the magnitude of noise is unknown, cross-validation

methods [24] could be useful.

The sophistication of our formulation is accompanied by its own set of challenges, including a complex optimization landscape and poor conditioning. For example, when data sets are large, noisy, and sparse, as seen in Example 5.2.2, the success of this method relies on an iterative solver, sometimes requiring an effective preconditioner for acceptable convergence rates. In this work we investigated many standard preconditioners (Incomplete Cholesky, Incomplete LU, Multi-Grid Methods, Jacobi) but failed to find a single, robust solution across the variety of problems. Further improvement of the optimization aspect of our approach will most likely require novel or bespoke methods.

Acknowledgements

The authors were supported through NSF award DMS-1908968. Additionally, TM was supported by the Department of Defense (DoD) through the National Defense Science & Engineering Graduate (NDSEG) Fellowship Program.

- [1] A. S. ACKLEH, R. R. FERDINAND, AND S. REICH, *Numerical studies of parameter estimation techniques for nonlinear evolution equations*, *Kybernetika*, 34 (1998), pp. 693–712.
- [2] H. AKAIKE, *Information theory and an extension of the maximum likelihood principle*, in *Selected Papers of Hirotugu Akaike*, E. Parzen, K. Tanabe, and G. Kitagawa, eds., Springer New York, New York, NY, 1998, pp. 199–213.
- [3] S. M. ALLEN AND J. W. CAHN, *A microscopic theory for antiphase boundary motion and its application to antiphase domain coarsening*, *Acta Metall.*, 27 (1979), pp. 1085–1095.
- [4] M. ASHYRALIYEV, J. JAEGER, AND J. G. BLOM, *Parameter estimation and determinability analysis applied to drosophila gap gene circuits*, *BMC Systems Biology*, 2 (2008), p. 83.
- [5] S. ATKINSON, W. SUBBER, L. WANG, G. KHAN, P. HAWI, AND R. GHANEM, *Data-driven discovery of free-form governing differential equations*, *arXiv preprint arXiv:1910.05117*, (2019).
- [6] D. A. BARAJAS-SOLANO AND A. M. TARTAKOVSKY, *Approximate bayesian model inversion for pdes with heterogeneous and state-dependent coefficients*, *Journal of Computational Physics*, 395 (2019), pp. 247–262.
- [7] J. BERG AND K. NYSTRÖM, *Neural network augmented inverse problems for pdes*, *arXiv preprint arXiv:1712.09685*, (2017).
- [8] J. BONGARD AND H. LIPSON, *Automated reverse engineering of nonlinear dynamical systems*, *Proceedings of the National Academy of Sciences*, 104 (2007), pp. 9943–9948.
- [9] C. BONNEVILLE AND C. EARLS, *Bayesian deep learning for partial differential equation parameter discovery with sparse and noisy data*, *Journal of Computational Physics: X*, 16 (2022), p. 100115.
- [10] G.-J. BOTH, S. CHOUDHURY, P. SENS, AND R. KUSTERS, *Deepmod: Deep learning for model discovery in noisy data*, *Journal of Computational Physics*, 428 (2021), p. 109985.
- [11] N. J. BRUNEL, *Parameter estimation of ode’s via nonparametric estimators*, *Electronic Journal of Statistics*, 2 (2008), pp. 1242–1267.
- [12] S. L. BRUNTON, J. L. PROCTOR, AND J. N. KUTZ, *Discovering governing equations from data by sparse identification of nonlinear dynamical systems*, *Proceedings of the national academy of sciences*, 113 (2016), pp. 3932–3937.

- [13] Y. CHEN, Y. LUO, Q. LIU, H. XU, AND D. ZHANG, *Symbolic genetic algorithm for discovering open-form partial differential equations (sga-pde)*, *Physical Review Research*, 4 (2022), p. 023174.
- [14] T. F. COLEMAN AND J. J. MORÉ, *Estimation of sparse hessian matrices and graph coloring problems*, *Math. Program.*, 28 (1984), pp. 243–270.
- [15] W. CROFT, C. M. ELLIOTT, G. LADDS, B. STINNER, C. VENKATARAMAN, AND C. WESTON, *Parameter identification problems in the modelling of cell motility*, *Journal of mathematical biology*, 71 (2015), pp. 399–436.
- [16] M. A. DEWAR, V. KADIRKAMANATHAN, M. OPPER, AND G. SANGUINETTI, *Parameter estimation and inference for stochastic reaction-diffusion systems: application to morphogenesis in d. melanogaster*, *BMC Systems Biology*, 4 (2010), p. 21.
- [17] R. FLETCHER AND C. M. REEVES, *Function minimization by conjugate gradients*, *Comput. J.*, 7 (1964), pp. 149–154.
- [18] J. FULLANA, P. LE GAL, M. ROSSI, AND S. ZALESKI, *Identification of parameters in amplitude equations describing coupled wakes*, *Physica D: Nonlinear Phenomena*, 102 (1997), pp. 37–56.
- [19] M. R. GARVIE, P. K. MAINI, AND C. TRENCHER, *An efficient and robust numerical algorithm for estimating parameters in turing systems*, *Journal of Computational Physics*, 229 (2010), pp. 7058–7071.
- [20] A. H. GEBREMEDHIN, F. MANNE, AND A. POTHEN, *What color is your jacobian? graph coloring for computing derivatives*, *SIAM Rev.*, 47 (2005), pp. 629–705.
- [21] K. GLASNER, *Optimization algorithms for parameter identification in parabolic partial differential equations*, *Computational and Applied Mathematics*, 40 (2021), p. 146.
- [22] ———, *Data-driven learning of differential equations: combining data and model uncertainty*, *Computational and Applied Mathematics*, 42 (2023), p. 36.
- [23] K. GLASNER AND S. ORIZAGA, *Improving the accuracy of convexity splitting methods for gradient flow equations*, *Journal of Computational Physics*, 315 (2016), pp. 52–64.
- [24] G. H. GOLUB, M. HEATH, AND G. WAHBA, *Generalized cross-validation as a method for choosing a good ridge parameter*, *Technometrics*, 21 (1979), pp. 215–223.
- [25] S. GUGUSHVILI AND C. A. KLAASSEN, *\sqrt{n} -consistent parameter estimation for systems of ordinary differential equations: bypassing numerical integration via smoothing*, *Bernoulli*, 18 (2012), pp. 1061–1098.
- [26] M. HARING, E. I. GROTLI, S. RIEMER-SORENSEN, K. SEEL, AND K. G. HANSSSEN, *A levenberg-marquardt algorithm for sparse identification of dynamical systems*, *IEEE Transactions on Neural Networks and Learning Systems*, (2022).
- [27] S. M. HIRSH, D. A. BARAJAS-SOLANO, AND J. N. KUTZ, *Sparsifying priors for bayesian uncertainty quantification in model discovery*, *Royal Society Open Science*, 9 (2022), p. 211823.
- [28] B. JIN AND P. MAASS, *Sparsity regularization for parameter identification problems*, *Inverse Problems*, 28 (2012), p. 123001.
- [29] G. E. KARNIADAKIS, I. G. KEVREKIDIS, L. LU, P. PERDIKARIS, S. WANG, AND L. YANG, *Physics-informed machine learning*, *Nature Reviews Physics*, 3 (2021), pp. 422–440.
- [30] D. P. KINGMA AND J. BA, *Adam: A method for stochastic optimization*, *arXiv preprint arXiv:1412.6980*, (2014).
- [31] E. KIYANI, S. SILBER, M. KOOSHKBAGHI, AND M. KARTTUNEN, *Machine-learning-based data-driven discovery of nonlinear phase-field dynamics*, *Physical Review E*, 106 (2022), p. 065303.

- [32] Y. KURAMOTO AND T. TSUZUKI, *On the formation of dissipative structures in reaction-diffusion systems: Reductive perturbation approach*, *Progr. Theoret. Phys.*, 54 (1975), pp. 687–699.
- [33] K. LEVENBERG, *A method for the solution of certain non-linear problems in least squares*, *Quart. Appl. Math.*, 2 (1944), pp. 164–168.
- [34] H. LIANG AND H. WU, *Parameter estimation for differential equation models using a framework of measurement error in regression models*, *Journal of the American Statistical Association*, 103 (2008), pp. 1570–1583.
- [35] D. C. LIU AND J. NOCEDAL, *On the limited memory bfgs method for large scale optimization*, *Math. Program.*, 45 (1989), pp. 503–528.
- [36] Z. LONG, Y. LU, AND B. DONG, *Pde-net 2.0: Learning pdes from data with a numeric-symbolic hybrid deep network*, *Journal of Computational Physics*, 399 (2019), p. 108925.
- [37] E. N. LORENZ, *Deterministic nonperiodic flow*, *J. Atmos. Sci.*, 20 (1963), pp. 130–141.
- [38] N. M. MANGAN, J. N. KUTZ, S. L. BRUNTON, AND J. L. PROCTOR, *Model selection for dynamical systems via sparse regression and information criteria*, *Proceedings of the Royal Society A: Mathematical, Physical and Engineering Sciences*, 473 (2017), p. 20170009.
- [39] D. W. MARQUARDT, *An algorithm for least-squares estimation of nonlinear parameters*, *Journal of the Society for Industrial and Applied Mathematics*, 11 (1963), pp. 431–441.
- [40] M. MASLYAEV, A. HVATOV, AND A. V. KALYUZHNAJA, *Partial differential equations discovery with epde framework: Application for real and synthetic data*, *Journal of Computational Science*, 53 (2021), p. 101345.
- [41] D. A. MESSENGER AND D. M. BORTZ, *Weak sindy for partial differential equations*, *Journal of Computational Physics*, 443 (2021), p. 110525.
- [42] H. MOHIMANI, M. BABAIE-ZADEH, AND C. JUTTEN, *A Fast Approach for Overcomplete Sparse Decomposition Based on Smoothed ^{0S} Norm*, *IEEE Transactions on Signal Processing*, 57 (2009), pp. 289–301. Conference Name: IEEE Transactions on Signal Processing.
- [43] V. MOROZOV, *On the solution of functional equations by the method of regularization*, *Dokl. Math.*, (1966).
- [44] J. NOCEDAL AND S. WRIGHT, *Numerical optimization*, *Springer Series in Operations Research and Financial Engineering*, Springer Nature, 2006.
- [45] M. J. D. POWELL AND P. L. TOINT, *On the estimation of sparse hessian matrices*, *SIAM J. Numer. Anal.*, 16 (1979), pp. 1060–1074.
- [46] M. RAISSI AND G. E. KARNIADAKIS, *Hidden physics models: Machine learning of nonlinear partial differential equations*, *Journal of Computational Physics*, 357 (2018), pp. 125–141.
- [47] M. RAISSI, P. PERDIKARIS, AND G. E. KARNIADAKIS, *Machine learning of linear differential equations using gaussian processes*, *Journal of Computational Physics*, 348 (2017), pp. 683–693.
- [48] M. RAISSI, P. PERDIKARIS, AND G. E. KARNIADAKIS, *Physics-informed neural networks: A deep learning framework for solving forward and inverse problems involving nonlinear partial differential equations*, *Journal of Computational Physics*, 378 (2019), pp. 686–707.
- [49] J. RAMSAY AND G. HOOKER, *Dynamic data analysis*, Springer, 2017.
- [50] J. O. RAMSAY, G. HOOKER, D. CAMPBELL, AND J. CAO, *Parameter estimation for differential equations: a generalized smoothing approach*, *Journal of the Royal Statistical Society: Series B (Statistical Methodology)*, 69 (2007), pp. 741–796.

- [51] J. O. RAMSAY AND B. W. SILVERMAN, *Fitting differential equations to functional data: Principal differential analysis*, Springer, 2005.
- [52] P. A. REINBOLD, D. R. GUREVICH, AND R. O. GRIGORIEV, *Using noisy or incomplete data to discover models of spatiotemporal dynamics*, *Physical Review E*, 101 (2020), p. 010203.
- [53] S. H. RUDY, S. L. BRUNTON, J. L. PROCTOR, AND J. N. KUTZ, *Data-driven discovery of partial differential equations*, *Science Advances*, 3 (2017), p. e1602614.
- [54] H. SCHAEFFER, *Learning partial differential equations via data discovery and sparse optimization*, *Proceedings of the Royal Society A: Mathematical, Physical and Engineering Sciences*, 473 (2017), p. 20160446.
- [55] M. SCHMIDT AND H. LIPSON, *Distilling free-form natural laws from experimental data*, *science*, 324 (2009), pp. 81–85.
- [56] G. SCHWARZ, *Estimating the dimension of a model*, *aos*, 6 (1978), pp. 461–464.
- [57] I. SGURA, A. S. LAWLESS, AND B. BOZZINI, *Parameter estimation for a morphochemical reaction-diffusion model of electrochemical pattern formation*, *Inverse Problems in Science and Engineering*, 27 (2019), pp. 618–647.
- [58] T. STEihaug, *The conjugate gradient method and trust regions in large scale optimization*, *SIAM J. Numer. Anal.*, 20 (1983), pp. 626–637.
- [59] R. STEPHANY AND C. EARLS, *Pde-learn: Using deep learning to discover partial differential equations from noisy, limited data*, *arXiv preprint arXiv:2212.04971*, (2022).
- [60] ———, *Pde-read: Human-readable partial differential equation discovery using deep learning*, *Neural Networks*, 154 (2022), pp. 360–382.
- [61] A. TIKHONOV, *Regularization of incorrectly posed problems*, 4 (1963), pp. 1624–1627.
- [62] ———, *Solution of incorrectly formulated problems and the regularization method*, *Sov Dok*, 5 (1963), pp. 1035–1038.
- [63] S.-M. UDRESCU AND M. TEGMARK, *Ai feynman: A physics-inspired method for symbolic regression*, *Science Advances*, 6 (2020), p. eaay2631.
- [64] H. U. VOSS, J. TIMMER, AND J. KURTHS, *Nonlinear dynamical system identification from uncertain and indirect measurements*, *International Journal of Bifurcation and Chaos*, 14 (2004), pp. 1905–1933.
- [65] H. XU, D. ZHANG, AND J. ZENG, *Deep-learning of parametric partial differential equations from sparse and noisy data*, *Physics of Fluids*, 33 (2021), p. 037132.
- [66] N. YOSHINAGA AND S. TOKUDA, *Bayesian modelling of pattern formation from one snapshot of pattern*, *arXiv preprint arXiv:2006.06125*, (2020).
- [67] H. ZHAO, R. D. BRAATZ, AND M. Z. BAZANT, *Image inversion and uncertainty quantification for constitutive laws of pattern formation*, *Journal of Computational Physics*, 436 (2021), p. 110279.
- [68] H. ZHAO, B. D. STOREY, R. D. BRAATZ, AND M. Z. BAZANT, *Learning the physics of pattern formation from images*, *Physical Review Letters*, 124 (2020), p. 060201.